annalen der physik
www.ann-phys.org

Energy and Matter Supply for Active Droplets

Jonathan Bauermann, Christoph A. Weber, and Frank Jülicher**

Chemically active droplets provide simple models for cell-like systems that can grow and divide. Such active droplet systems are driven away from thermodynamic equilibrium and turn over chemically, which corresponds to a simple metabolism. Two scenarios of nonequilibrium driving are considered. First, droplets are driven via the system boundaries by external reservoirs that supply nutrient and remove waste (boundary-driven). Second, droplets are driven by a chemical energy provided by a fuel in the bulk (bulk-driven). For both scenarios, the conservation of energy and matter as well as the balance of entropy are discussed. Conserved and nonconserved fields are used to analyse the nonequilibrium steady states of active droplets. Using an effective droplet model, droplet stability and instabilities leading to droplet division are explored. This work reveals that droplet division occurs quite generally in active droplet systems. The results suggest that life-like processes such as metabolism and division can emerge in simple nonequilibrium systems that combine the physics of phase separation and chemical reactions.

1. Introduction

Chemical processes in living cells are organized in distinct compartments. Some of these compartments use membranes, others use interfaces that separate coexisting phases.[1–4] An important question is how compartmentalization provided by droplets affects chemical processes[5–8] It has already been proposed 100 years ago that chemical compartmentalization by phase-separated coacervates could have played a key role at the origin of life.[9–12] In particular, phase-separated droplets could serve as simple models of protocells with life-like behaviors when maintained away from equilibrium:

(i) Droplets enrich and confine certain components providing a distinct chemical environment.
(ii) Such droplets can localize chemical reactions defining a proto-metabolism.
(iii) Chemical activity can drive droplet growth.
(iv) Chemically active droplets can undergo a shape instability, and divide into daughter droplets. The life-life behaviors (i)–(iv) have been discussed theoretically using minimal models as a proof of principle[13–15] Such minimal models, however, consider simple binary mixtures that are composed of two components which undergo demixing and also can chemically convert into each other—a simplification that can be hardly realized in experimental chemical system.

In this work, we discuss more realistic scenarios of droplet models of protocells. These scenarios distinguish between nutrient, droplet material, waste, and solvent. Such systems are versatile and open new possibilities for experimental realizations since real chemical systems with active droplets[16–19] are not binary and the spatial distribution of nutrients and waste is in general relevant for the emergence of the aforementioned life-like behaviors. Droplet systems also provide appealing models of simple but realistic protocells and permit to consider both energy and matter flows.

The paper is organized as follows. In Section 2, we first introduce two complementary cases of active droplets which provide models of protocells which differ in the supply of matter and energy. In Section 3, building upon recently developed theoretical concepts,[8,15,20] we present a general theory of droplet systems in the presence of chemical reactions. We use this approach in Section 4 to discuss the dynamics of protocells for the two cases. In Section 5, we discuss the energy, mass, and entropy balance in these systems and we discuss our results in Section 6.

2. Active Droplet Models of Simple Protocells

We introduce active droplet models based on four components, $i = S, D, N, W$. These components are solvent S, droplet material

J. Bauermann, F. Jülicher
Max Planck Institute for the Physics of Complex Systems
Nöthnitzer Straße 38, 01187 Dresden, Germany
E-mail: julicher@pks.mpg.de
C. A. Weber
Faculty of Mathematics
Natural Sciences, and Materials Engineering: Institute of Physics
University of Augsburg
Universitätsstraße 1, 86159 Augsburg, Germany
E-mail: christoph.weber@physik.uni-augsburg.de
F. Jülicher
Center for Systems Biology Dresden
Pfotenhauerstrasse 108, 01307 Dresden, Germany
F. Jülicher
Cluster of Excellence Physics of Life
TU Dresden, 01062 Dresden, Germany

The ORCID identification number(s) for the author(s) of this article can be found under https://doi.org/10.1002/andp.202200132

DOI: 10.1002/andp.202200132

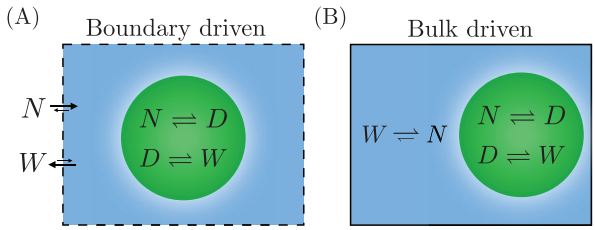

Figure 1. Chemical reactions maintained away from equilibrium by reservoirs of nutrient and waste. A) Boundary-driven case with nutrient and waste reservoirs at the system boundary. B) Bulk-driven case with energy supply via chemical reactions with broken detailed balance in the outside phase.

D, nutrient N, and waste W. We first specify the components involved in phase separation and introduce the chemical reactions. We then discuss the conditions by which the system is driven out of thermodynamic equilibrium.

2.1. Phase Separation and Chemical Reactions

We consider an incompressible, phase-separating system that undergoes chemical reactions, see **Figure 1**. Droplet material D phase-separates from a solvent S leading to droplets. A nutrient component N can chemically convert to droplet material D, thereby feeding the droplet. Droplet material can undergo a chemical change to become waste W. These reactions can be written as

$$N \rightleftharpoons D \quad (\alpha = 1) \tag{1}$$

$$D \rightleftharpoons W \quad (\alpha = 2) \tag{2}$$

and are indexed with $\alpha = 1, 2$. For simplicity, we consider that reactions involving the droplet material only occur inside the droplets. This is motivated by the idea that these reactions are enabled by catalysts that are absent outside and thus solely located inside droplets. We also consider the possibility that waste W can be directly converted to nutrient N.

This reaction can be written as

$$W \rightleftharpoons N \quad (\alpha = 3) \tag{3}$$

This reaction, for simplicity, only occurs outside of the droplet.

2.2. Energy and Matter Supply

In order to discuss the energy balance, we need to introduce the exchange chemical potentials μ_D, μ_N, and μ_W with respect to the solvent component. We discuss two different cases of nonequilibrium driving, boundary-driven and bulk-driven, see Figure 1A,B.

In the boundary driven case (A), the concentrations of nutrient N, waste W and droplet material D at the system boundary are fixed via concentration boundary conditions, corresponding to a coupling to a reservoir. This reservoir set values of the chemical potentials at the boundary μ_i^∞. We choose conditions where $\mu_N^\infty > \mu_D^\infty > \mu_W^\infty$ such that the direction of chemical reactions is from nutrient via droplet material to waste. Therefore, nutrient will be provided and waste will be absorbed by the reservoir. In this case, we do not consider the direct reaction between waste and nutrient Equation (3). In this case (A), the free energy provided by the reservoir per consumed nutrient molecule is $\mu_N^\infty - \mu_W^\infty > 0$. This difference maintains the system out of equilibrium and drives a constant flux of molecules through the system. The total volume fraction $\psi = \phi_D + \phi_N + \phi_W$, where ϕ_i denotes the volume fraction of component i, is a conserved quantity. It obeys the continuity equation, $\partial_t \psi + \nabla \cdot \boldsymbol{j}_\psi = 0$, where $\boldsymbol{j}_\psi$ is the associated, conserved current. The conserved quantity is provided by the reservoir and can feed droplet growth. Therefore, droplet size is not limited by the conservation law.

In the bulk driven case (B), we impose no-flux boundary conditions, considering that no exchange of molecules with reservoirs occurs at the boundaries. The system is maintained out-of-equilibrium by introducing an external energy input $\Delta\mu^{\text{act}}$ to the reaction Equation (3) ($\alpha = 3$). This energy input could, for example, be provided by chemical fuel or by radiation. The energy input $\Delta\mu^{\text{act}}$ drives the reaction which would spontaneously run from N to W in the opposite direction and allows nutrient to be recycled to waste. This can be achieved when $\Delta\mu^{\text{act}} + \mu_W > \mu_N$. The quantity ψ is again a conserved quantity. Since there is no exchange at the boundaries, the amount of this conserved quantity ψ is fixed inside the system. Therefore, the amount of droplet material D is limited by the conserved quantity. This is implied that even though free energy $\Delta\mu^{\text{act}}$ is continuously supplied to the system, the droplet size is limited by the conservation law.

2.3. Droplet Dynamics and Droplet Division

These cases can be compared to the minimal protocell model based on a binary system studied previously.[14] In this simple system, two components phase-separate from each other and can also be chemical converted into each other. Active droplets in this binary system are driven in the bulk by the chemical energy input $\Delta\mu^{\text{act}}$. However, in this binary system, there is only one independent volume fraction and no conservation law. Therefore, droplet size is not limited by a conservation law. In previous work,[14] it was shown that droplets can either shrink and disappear, grow until droplets reach a stable size or undergo a shape instability and divide. In the latter case, cycles of growth and division can lead to many daughter droplets that together occupy an increasing volume.

Motivated by these findings, we study here the dynamics and properties of active droplets in the more realistic protocell models introduced here. These models differ from the binary model by taking into account a solvent S which phase-separates from the droplet material D. Most importantly, this solvent does not undergo chemical transitions with the droplet material D. Therefore, the proposed models in our work are closer to existing experimental systems.[16–19]

As we will show in the following, our simple protocell models also exhibit regimes where droplets are stable with a finite size, and regimes where droplets divide via a shape instability. Examples of droplet dynamics in the boundary driven case are shown in **Figure 2** as snapshots of configurations of droplet material at

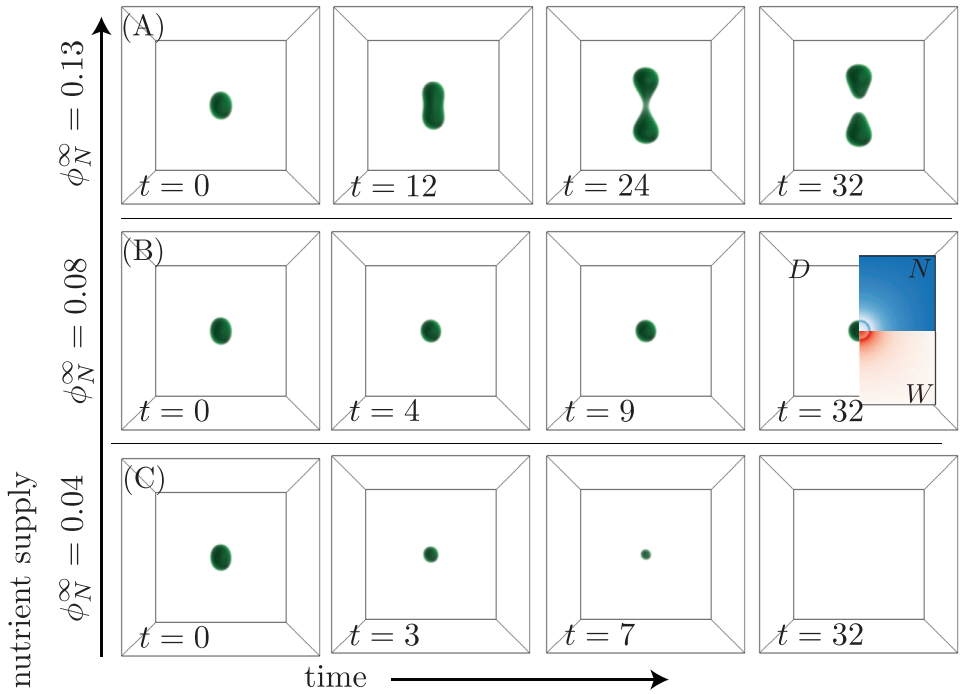

Figure 2. Shape dynamics of active droplets. A–C) Volume fraction fields of droplet material ϕ_D for different time points t in boundary-driven systems for three values of ϕ_N as indicated. Last panel in (B) shows density distributions of ϕ_N and ϕ_W on a planar cross section. Solutions were obtained by numerical integration of Equation (4), initializing with a slightly elongated droplet at $t = 0$. Parameter values are given in Table C1 and Appendix C.

different time points and for different nutrient reservoir volume fractions ϕ_N^∞. For all cases, we initialize an almost spherical droplet with small shape elongation that is positioned at the system center. For small nutrient supply ($\phi_N^\infty = 0.04$), an initially prepared droplet tends to shrink as the waste release from the droplets exceeds the nutrient supply. In this case, the rate of nutrient supply set by the boundary conditions, which leads to generation of new droplet material is insufficient to compensate for droplet material loss via its transition to waste, which leaves the system at the boundaries. For larger nutrient supply ($\phi_N^\infty = 0.08$), an active droplet is stationary with a size that is determined by the nutrient supply. At this stationary state, the transition of nutrient to droplet material within the droplet balances the loss of droplet material transitioning to waste. Increasing the nutrient supply further ($\phi_N^\infty = 0.13$), the spherical shape becomes unstable with respect to small perturbations and droplet division occurs. These different cases will be discussed in more detail in Sections 4 and 5.

In the next chapter we present the general theory of multicomponent active droplets and discuss in detail the energetics and the conservation laws.

3. Theory of Chemically Active Droplets

In this section, we derive the theory for chemically active droplets using nonequilibrium thermodynamics; for a discussion of homogeneous, nondilute mixtures with chemical reactions, see ref. [21]. The dynamics of such systems are governed by chemical potential differences .[15] In the case of active droplets, these chemical potentials determine both the thermodynamics of phase separation and the thermodynamics of chemical reactions.

3.1. Irreversible Thermodynamics of Phase Separation and Reactions

We consider an incompressible mixture of $M + 1$ chemical components, denoted as C_i, with $i = 0, \dots, M$. The local composition is given by the volume fractions ϕ_i with $i = 1, \dots, M$ indicating the different components. The volume fraction ϕ_0, which we identify with the solvent S, is not an independent variable, because of the constraint $\sum_{i=0}^{M} \phi_i = 1$. The volume fractions are related to the local concentrations n_i via $\phi_i = v_i n_i$, where v_i is the molecular volume of components i. Incompressibility implies that the molecular volumes v_i are constant parameters at constant temperature. The dynamical equations for the volume fractions read

$$\partial_t \phi_i = -\nabla \cdot \boldsymbol{j}_i + r_i \tag{4}$$

where $\boldsymbol{j}_i$ is a diffusive current of volume fraction and r_i denote source and sink terms resulting from chemical reactions. Incompressibility requires that chemical reactions conserve volume, which implies $\sum_{i=0}^{M} r_i = 0$.

The diffusive flux arises due to spatial gradients of the exchange chemical potentials $\mu_i = v_i \delta F / \delta \phi_i$, where $F[\phi_1, \dots, \phi_M]$ is the free energy and $\delta F / \delta \phi_i$ denotes a functional derivative. In general, we can write

$$\mu_i = k_B T \log(\gamma_i \phi_i) + \omega_i - \kappa_i \nabla^2 \phi_i \tag{5}$$

where $(\gamma_i \phi_i)$ is the exchange activity of components i relative to the solvent, γ_i is the corresponding activity coefficient and ω_i are

the reference chemical potentials. For mean-field models up to the second virial coefficients, the activity coefficient has the form

$$\gamma_i = \phi_0^{-\frac{\nu_i}{\nu_0}} \exp\left(\nu_i \frac{\sum_{j=1}^{M}(\chi_{ij} - \chi_{i0} - \chi_{j0})\phi_j}{k_B T}\right) \tag{6}$$

where the matrix χ_{ij} describes the molecular interactions, see Appendix A. The contribution ω_k is independent of composition and corresponds to a reference chemical potential. Furthermore, k_B is the Boltzmann constant and T temperature. The coefficient κ_i characterizes the free energy contributions due to gradients of composition and is related to interfacial tension.

The diffusive flux of volume fraction is driven by chemical potential gradients

$$\boldsymbol{j}_i = -\nu_i \sum_{j=1}^{M} \Lambda_{ij} \nabla \mu_j \tag{7}$$

where Λ_{ij} denotes the mobility matrix with $\Lambda_{ij} = \Lambda_{ji}$. For simplicity, we choose $\Lambda_{ij} = \lambda \phi_i(\delta_{ij} - \phi_j)$, where λ is a molecular mobility. The diffusion matrix is then given by

$$D_{ij} = \nu_i \sum_{k=1}^{M} \Lambda_{ik} \frac{\partial \mu_k(\phi)}{\partial \phi_j} \tag{8}$$

which becomes diagonal $D_{ij} = k_B T \lambda \delta_{ij}$ for vanishing molecular interactions and all molecular volumes being equal, $\nu_i = \nu$. Thus, all molecular components diffusive independently of each other with the same diffusion coefficient.

The source rate r_i of component i in Equation (4) stems from chemical reactions. Each chemical reaction $\alpha = 1, \ldots, L$ can be written as

$$\sum_{i=0}^{M} \sigma_{i\alpha}^{+} C_i \underset{r_\alpha^-}{\overset{r_\alpha^+}{\rightleftharpoons}} \sum_{i=0}^{M} \sigma_{i\alpha}^{-} C_i \tag{9}$$

where C_i is the chemical symbol of components i and $\sigma_{i\alpha}^{\pm}$ are stoichiometric coefficients. The net chemical rate per volume $r_\alpha = r_\alpha^+ - r_\alpha^-$ can be written as a difference of the forward and backward rates. We also define the stoichiometric matrix $\sigma_{i\alpha} = \sigma_{i\alpha}^- - \sigma_{i\alpha}^+$.

The relation between the source rates r_i and the chemical rates r_α reads

$$r_i = \sum_{\alpha=1}^{S} \nu_i \sigma_{i\alpha} r_\alpha \tag{10}$$

and the stoichiometric coefficients $\sigma_{i\alpha}$ for volume conserving reactions must obey

$$\sum_{i=0}^{M} \nu_i \sigma_{i\alpha} = 0 \tag{11}$$

The chemical reactions are driven by the reaction Gibbs free energy

$$\Delta\mu_\alpha = \sum_{i=1}^{M} \sigma_{i\alpha} \mu_i \tag{12}$$

which can be expressed in terms of the exchange chemical potential μ_i given in Equation (5). The Gibbs free energy is the free energy change associated with a single event of reaction α. Microscopic reversibility imposes a detailed balance condition for forward and backward rates

$$\frac{r_\alpha^+}{r_\alpha^-} = \exp\left(-\frac{\Delta\mu_\alpha}{k_B T}\right) \tag{13}$$

This condition ensures that the system relaxes toward thermodynamic equilibrium in the absence of driving. Chemical rates that satisfy this detailed balance condition can in general be written as

$$r_\alpha^{\pm} = k_\alpha \exp\left(\frac{\sum_{i=1}^{M} \sigma_{i\alpha}^{\pm} \mu_i}{k_B T}\right) \tag{14}$$

where k_α is a kinetic coefficient. The kinetics of the reactions is specified by the values and composition dependence of the kinetic coefficients k_α. We will use the freedom to choose this dependence of k_α on ϕ_i to localize reactions either inside or outside of droplets.

Substituting the exchange chemical potentials (5) in the relation of the source rate (10) gives

$$r_i = \sum_{\alpha=1}^{S} k_\alpha \sigma_{i\alpha} \nu_i \left(\prod_{n=0}^{M} (\rho_n \phi_n)^{\sigma_{n\alpha}^+} - \prod_{n=0}^{M} (\rho_n \phi_n)^{\sigma_{n\alpha}^-}\right) \tag{15}$$

where

$$\rho_n = \gamma_n \exp\left(\frac{\omega_n - \kappa_n \nabla^2 \phi_n}{k_B T}\right) \tag{16}$$

In dilute and homogeneous systems, ρ_n are constant parameters, while in phase-separated systems, the coefficients ρ_n depend on composition.

3.2. Conserved and Nonconserved Densities

The volume fractions ϕ_i are not conserved, which follows from the presence of the source rates r_i in the balance equation (4). In general, there are $L' \leq M$ linearly independent chemical reactions. Therefore, there remain $C = M - L'$ conserved densities in addition to the conserved volume. These conserved densities can be expressed as linear combinations of volume fractions. We write the conserved densities as

$$\psi_j = \sum_{i=0}^{M} A_{ji} \phi_i \tag{17}$$

where $j = 0, 1, \ldots, C$. Here, the matrix $\underline{\underline{A}}$ obeys the relation $\sum_{i=0}^{M} A_{ji} \nu_i \sigma_{i\alpha} = 0$, that is, the rows of the matrix $\underline{\underline{A}}$ are linearly independent null-vectors of the matrix $\nu_i \sigma_{i\alpha}$. The conservation law Equation (11) corresponds to $j = 0$ with $A_{0i} = 1/\nu_0$, which also

clarifies that the units of ψ_j are inverse volume. We can also define the $L' = M - C$ non-conserved densities

$$\xi_\alpha = \sum_{0=1}^{M} B_{\alpha i}\phi_i \tag{18}$$

where $\alpha = 1, \ldots, L'$, which are the extents of reactions. The reaction extents ξ_α measure the cumulative number of reaction events that have occurred per volume. Here, the densities ψ_j and ξ_α obey

$$\partial_t \psi_j = -\nabla \cdot \boldsymbol{j}_j^{\psi} \tag{19a}$$

$$\partial_t \xi_\alpha = -\nabla \cdot \boldsymbol{j}_\alpha^{\xi} + r_\alpha \tag{19b}$$

where we introduce the currents $\boldsymbol{j}_j^{\psi} = \sum_{i=0}^{M} A_{ji}\boldsymbol{j}_i$ of the conserved densities and the extent currents and $\boldsymbol{j}_\alpha^{\xi} = \sum_{i=0}^{M} B_{\alpha i}\boldsymbol{j}_i$. Note that volume conservation corresponds to $\psi_0 = \sum_{i=0}^{M} \phi_i/\nu_0 = 1/\nu_0$ is not a dynamical variable and $j_0^{\psi} = 0$.

The matrices $\underline{\underline{A}}$ and $\underline{\underline{B}}$ define the matrix elements of an invertible square matrix

$$\underline{\underline{U}} = \begin{pmatrix} A_{00} & \cdots & A_{0i} & \cdots & A_{0M} \\ & \cdots & A_{ji} & \cdots & \\ A_{C0} & \cdots & A_{Ci} & \cdots & A_{CM} \\ B_{1i} & \ldots & B_{1i} & \ldots & B_{1M} \\ & \cdots & B_{\alpha i} & \cdots & \\ B_{L'0} & \cdots & B_{L'i} & \ldots & B_{L'M} \end{pmatrix} \tag{20}$$

A property of the inverse matrix $\underline{\underline{U}}^{-1}$ is $\underline{\underline{U}}^{-1}_{i\alpha} = \nu_i\sigma_{i\alpha}$. Note that the matrix $\underline{\underline{A}}$ and the conserved densities ψ_j are not unique. Any linear combination of conserved densities is also a conserved density. A choice of linearly independent conserved densities specifies the matrix $\underline{\underline{A}}$ uniquely. Similarly, the matrix $\underline{\underline{B}}$ is also not unique, because each reaction extent is defined with respect to a reference value.

From the conserved densities ψ_j and the reaction extents ξ_α, we can obtain the volume fractions,

$$\phi_i = \sum_{j=0}^{C} U_{ij}^{-1}\psi_j + \sum_{\alpha=1}^{L'} \nu_i\sigma_{i\alpha}\xi_\alpha \tag{21}$$

3.3. Energetics and Entropy Production

We now discuss the energetics and thermodynamics of chemically active droplets. The free energy of the system, $F = \int d^3x f$, from which we derive the chemical potential (5), can be expressed in terms of the free energy density f. The density of internal energy, $e = f + Ts$, can be decomposed into the free energy density and an entropy density $s = -\partial f/\partial T$. Energy conservation can be written as

$$\partial_t e + \nabla \cdot \boldsymbol{j}_h = -\nabla \cdot \boldsymbol{j}_q \tag{22}$$

where we decompose the flux of energy into a heat flux $\boldsymbol{j}_q$ and an enthalpy flux $\boldsymbol{j}_h$. Note that Equation (22) defines the heat flux. For simplicity, we focus on isothermal systems at constant temperature T. The heat flux is determined by the constraint of fixed temperature, which corresponds to the limit of large heat conductance.

The flux of enthalpy is given as $\boldsymbol{j}_h = \sum_{i=1}^{M} h_i\boldsymbol{j}_i/\nu_i$, where we define the enthalpy $h_i = \mu_i + Ts_i$ per molecule C_i with $s_i = -\partial\mu_i/\partial T$ denoting the entropy per molecule.

The rate of change of internal energy density reads $\partial_t e = \sum_{i=1}^{M} h_i\partial_t\phi_i/\nu_i$. Using Equation (22), we can identify the heat production rate as

$$\nabla \cdot \boldsymbol{j}_q = -\sum_{\alpha=1}^{L'} r_\alpha \Delta h_\alpha - \sum_{i=1}^{M} \frac{\boldsymbol{j}_i}{\nu_i} \cdot \nabla h_i \tag{23}$$

where $\Delta h_\alpha = \sum_{i=1}^{M} \sigma_{i\alpha} h_i$ is the reaction enthalpy. Using the definitions of the entropy density s and energy density e, we obtain the entropy balance

$$\partial_t s + \nabla \cdot \boldsymbol{j}_s = \dot{\Theta} \tag{24}$$

where the entropy flux is $\boldsymbol{j}_s = \sum_{i=1}^{M} s_i\boldsymbol{j}_i/\nu_i + \boldsymbol{j}_q/T$. The entropy production rate $\dot{\Theta}$ obeys

$$T\dot{\Theta} = -\sum_{\alpha=1}^{L'} r_\alpha \Delta\mu_\alpha - \sum_{i=1}^{M} \frac{\boldsymbol{j}_i}{\nu_i} \cdot \nabla\mu_i \tag{25}$$

which is zero or positive according to the second law of thermodynamics.

In summary, we have derived a complete description for phase-separated systems in the presence of chemical reactions at constant temperature. The system is captured by C conserved quantities ψ, and L' reaction extents ξ, described by Equation (19a) and Equation (19b) and obeys the energy conservation, as well as heat and entropy production are described by Equations (23) and (25). Note that volume changes of coexisting phases are associated with conserved fluxes $\boldsymbol{j}^{\psi}$.

4. Dynamics of Protocells

In this section we specify the particular model introduced in Section 2.1 and study the dynamics of active droplets in the boundary and bulk driven cases, respectively.

4.1. Model Parameters

Molecular interactions are described by the matrix with elements χ_{ij}. We consider $M = 3$ nonsolvent components D, N, and W as well a solvent S. For simplicity, all molecular components have the same molecular volume $\nu_i = \nu$. The choice of interactions is based on the idea that droplet material phase-separates from the solvent. The matrix is symmetric and the diagonal elements can

be chosen to zero, $\chi_{ii} = 0$, without loss of generality. Thus, there are a six independent entries in the interaction matrix

$$\underline{\underline{\chi}} = \begin{array}{c} \begin{matrix} S & D & N & W \end{matrix} \\ \begin{pmatrix} 0 & \chi_{DS} & \chi_{NS} & \chi_{WS} \\ \chi_{DS} & 0 & \chi_{DN} & \chi_{DW} \\ \chi_{NS} & \chi_{DN} & 0 & \chi_{NW} \\ \chi_{WS} & \chi_{DW} & \chi_{NW} & 0 \end{pmatrix} \end{array} \begin{matrix} S \\ D \\ N \\ W \end{matrix} \tag{26}$$

For the chemical reactions depicted in Figure 1, we have $L = 3$ reactions out of which $L' = 2$ are linearly independent, see Equations (1)–(2). The stoichiometric matrix of the linear independent reactions $\alpha = 1$ and $\alpha = 2$ is given by

$$\underline{\underline{\sigma}} = \begin{array}{c} \begin{matrix} \alpha = 1 & \alpha = 2 \end{matrix} \\ \begin{pmatrix} 0 & 0 \\ 1 & -1 \\ -1 & 0 \\ 0 & 1 \end{pmatrix} \end{array} \begin{matrix} S \\ D \\ N \\ W \end{matrix} \tag{27}$$

Conserved densities ψ_j and reaction extents ξ_α are obtained from volume fractions via the transformation matrix

$$\underline{\underline{U}} = \nu^{-1} \begin{pmatrix} 1 & 1 & 1 & 1 \\ 0 & 1 & 1 & 1 \\ 0 & 0 & -1 & 0 \\ 0 & 1 & 1 & 2 \end{pmatrix} \tag{28}$$

see Equation (20). In addition to the volume conservation, the relevant conserved density $\psi = (\phi_D + \phi_N + \phi_W)/\nu$ describes the conservation of nonsolvent components. The reaction extent variables are $\xi_1 = -\phi_N/\nu$ and $\xi_2 = (\phi_D + \phi_N - 2\phi_W)/\nu$. The inverse transformation matrix is given by

$$\underline{\underline{U^{-1}}} = \nu \begin{pmatrix} 1 & -1 & 0 & 0 \\ 0 & 2 & 1 & -1 \\ 0 & 0 & -1 & 0 \\ 0 & -1 & 0 & 1 \end{pmatrix} \tag{29}$$

and obeys the equation $U^{-1}_{i\alpha} = \nu_i \sigma_{i\alpha}$.

Reaction rates are specified by kinetic coefficients k_α which depend on composition. In our model, the reactions $\alpha = 1, 2$ occur only inside the droplet phase with a rate

$$k_\alpha = \frac{K_\alpha}{2}\left(1 + \tanh\left(\frac{\phi_D - \Phi}{\epsilon}\right)\right) \tag{30}$$

where K_α is a rate constant. Moreover, Φ denotes a parameter corresponding to the value of the volume fraction ϕ_D at the interface between droplet phase and solvent phase, and $\epsilon > 0$ characterizes how much the reaction $\alpha = 1, 2$ is suppressed outside the droplet. In the bulk driven case, the reaction $\alpha = 3$ occurs outside the droplet, corresponding to $\epsilon < 0$. In addition, the system is driven by an external energy input $\Delta\mu^{\text{act}}$. Therefore, we use for $\alpha = 3$, instead of Equation (14), the following forward reaction rate

$$r_3^+ = k_3(\phi_D) \exp\left(\frac{\mu_W + \Delta\mu^{\text{act}}}{k_B T}\right) \tag{31}$$

and for rate of the backward reaction, we consider

$$r_3^- = k_3(\phi_D) \exp\left(\frac{\mu_N}{k_B T}\right) \tag{32}$$

4.2. Steady State Droplets

In order to characterize steady states of spherical droplets and their stability, we consider, for simplicity, the case of a sharp interface and an infinitely large system volume; see Appendix B. In this limit of a sharp interface, we obtain linear reaction–diffusion equations (B1) inside and outside the droplet. These equations are derived by linearization around the concentrations that coexist at the interface which is at local equilibrium. We impose boundary conditions at the interface that ensure currents across the interface being continuous at steady state. This continuity of currents selects an unique tie line which connects the coexisting concentrations in the phase diagram.

In the boundary driven case, we impose concentration boundary conditions at infinity with values ϕ_D^∞, ϕ_N^∞, and ϕ_W^∞ for the volume fractions of droplet material D, nutrient N, and waste W. Fixed concentration boundary conditions imply that material is supplied via net currents at infinity.

Figure 3A shows profiles of volume fractions of droplet material D, nutrient N, and waste W in the boundary driven case for a spherical droplet of size R as a function of the radial coordinate r. The droplet material is produced by reaction $\alpha = 1$ inside the droplet (gray region) where it is also the majority component. The droplet material also occurs outside at low concentrations. Nutrient is provided at large distances and diffuse toward the droplet. Waste is produced inside the droplet by the reaction $\alpha = 2$ and diffuses outward. The system is maintained out-of-equilibrium by the concentration boundary conditions at infinity, where $\mu_N \neq \mu_W$. Note that detailed balance is obeyed everywhere in the system.

Figure 3B shows the profiles of the conserved density ψ and the extent of the two reactions ξ_1, ξ_2 in the boundary driven case. The current of the conserved density vanishes, because the system is at steady state. The divergence of the extent currents $\nabla \cdot j_\alpha^\xi = r_\alpha$ indicate chemical activity at rate r_α. Note that outside the droplet, divergence-free extent currents occur without reactions. The steady state droplet radius depends on the concentrations imposed at infinity, see Figure 3C, which shows stationary radii of stable (solid lines) and unstable (dashed lines) droplets for two different values of ϕ_D^∞ as a function of ϕ_N^∞. Droplets nucleated beyond the critical radius (dashed lines) grow until they reach the stable stationary radius (solid lines), while droplets larger than the stable radius shrink. For smaller volume fractions ϕ_D^∞ droplet

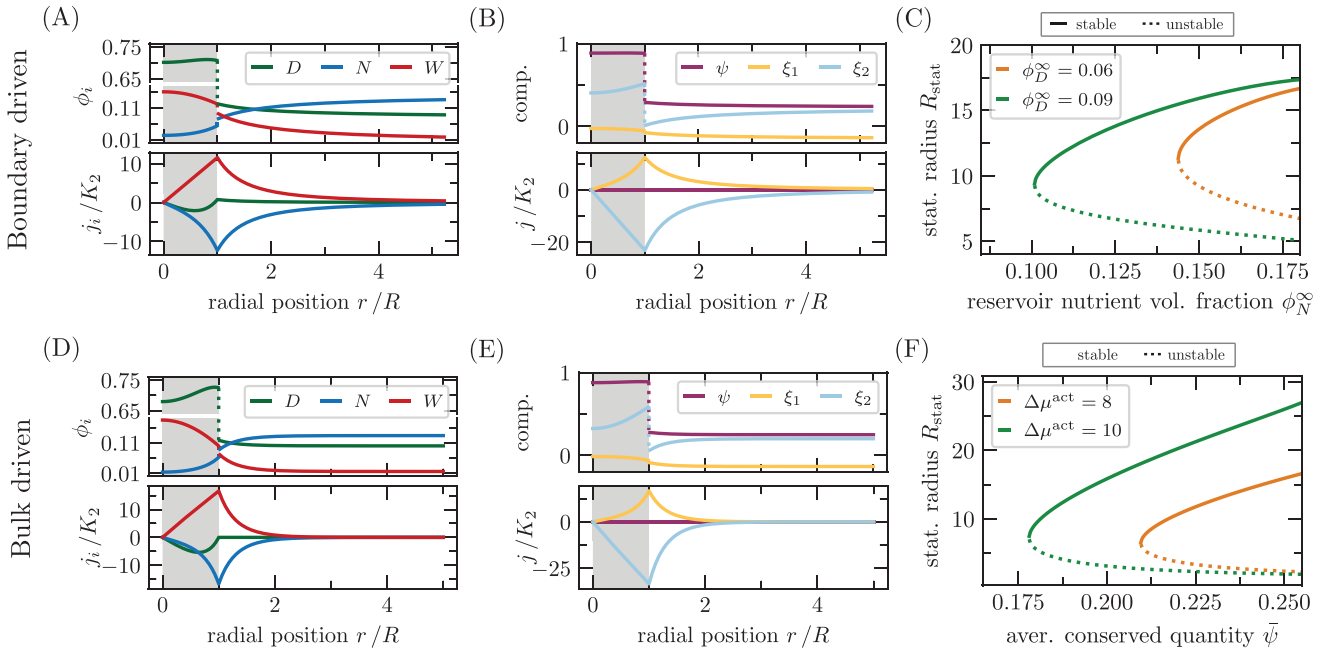

Figure 3. Stationary active droplets. Profiles of various quantities for the boundary-driven case (upper row) and the bulk-driven case (lower row). A,D) Profiles of volume fractions and corresponding diffusive fluxes for droplet material, nutrient and waste. B,E) Profiles of conserved density ξ and non-conserved reaction extents $\xi_{1/2}$ and their corresponding diffusive fluxes. Such profiles are obtained from Equations (19a) and (19b). C,F) Stable and unstable stationary radii R_{stat} of chemically active droplets. For the boundary-driven case, R_{stat} is shown as a function of the nutrient volume fraction of the reservoir ϕ_N^∞ for two different reservoir values of the droplet material ϕ_D^∞. For the bulk-driven case, R_{stat} is depicted as a function of the averaged conserved quantity $\bar{\psi}$ for two different values of external energy input $\Delta\mu^{\text{act}}$ (Equation (31)) that break detailed balance of the rates (13). The parameters of these systems are given in Parameter values are given in Table C1 and Appendix C.

material is lost by diffusion toward infinity, requiring larger volume fractions ϕ_N^∞ to maintain the droplet.

In the bulk driven case, we impose that no net current of the conserved quantity j^ψ exits at infinity. In addition, reaction $\alpha = 3$ is imposed at local chemical equilibrium with $\Delta\mu^{\text{act}} = \mu_N - \mu_W$, where $\Delta\mu^{\text{act}}$ is the chemical free energy supplied by a fuel. Note that, the reaction $\alpha = 3$ occurs outside of the droplet to regenerate nutrient from waste. The profiles of volume fractions of a steady state droplet are shown in Figure 3D, together with the corresponding currents. The profiles of volume fraction are qualitatively similar to the boundary driven case shown in Figure 3A. The main difference is that the currents decay more quickly and no net current remain at infinity. The corresponding conserved density and reaction extent are shown in Figure 3E.

The boundary driven case and the bulk driven case give similar profiles for the conserved density ψ and the reaction extents ξ_1 and ξ_2 (compare Figure 3A,B,D,E). A key difference is that the divergence of the extent currents, $\nabla \cdot j^\xi$, in the boundary driven case vanishes outside the droplets, while for the bulk driven case, this divergence is nonzero outside, corresponding to the rate of the reaction that produces nutrient. Note that the reaction in the bulk driven case cannot alter the amount of conserved material, therefore, the droplets growth is limited via the conserved material.

The stable and unstable radii of stationary droplets are shown in Figure 3F for the bulk driven case as a function of the conserved quantity ψ^∞ and for two different values of $\Delta\mu^{\text{act}}$. Increasing $\Delta\mu^{\text{act}}$ enables chemically active droplets for smaller values of the conserved quantity ψ^∞ and leads to larger stable stationary droplets. This behaviour is similar to that the boundary driven case, see Figure 3C. Increasing $\Delta\mu^{\text{act}}$ in the bulk driven case has the same qualitative effect on the stationary radius, as an increase of nutrient supply via ϕ_N^∞ in the boundary driven case, compare Figure 3C,F.

4.3. Droplet Stability

So far, we have considered stationary droplets of spherical shapes. Due to nonequilibrium conditions, chemically active droplets can also undergo a shape instability and take nonspherical shapes and thereby even divide. An example of a division event is shown in Figure 2A. We can systematically study the linear stability of spherical shapes using the sharp interface limit, see Appendix B.

In **Figure 4**A, we show a stability diagram of chemically active droplets for the boundary driven case as function of nutrient and droplet material volume fraction at infinity, ϕ_N^∞ and ϕ_D^∞, for fixed ϕ_W^∞. Stationary spherical droplets are stable within the green region of the diagram. Within the yellow region, a spherical harmonic deformation mode with $l = 2$ is unstable. This corresponds to an elongation of the droplet shape. Similarly, in the red region, a spherical deformation mode with $l = 3$ is also unstable. In the white region, no stationary droplets exit. The figure shows, that starting from a stationary stable droplet, division can typically be induced by increasing the supply of either nutrient or droplet material. The binodal line of phase

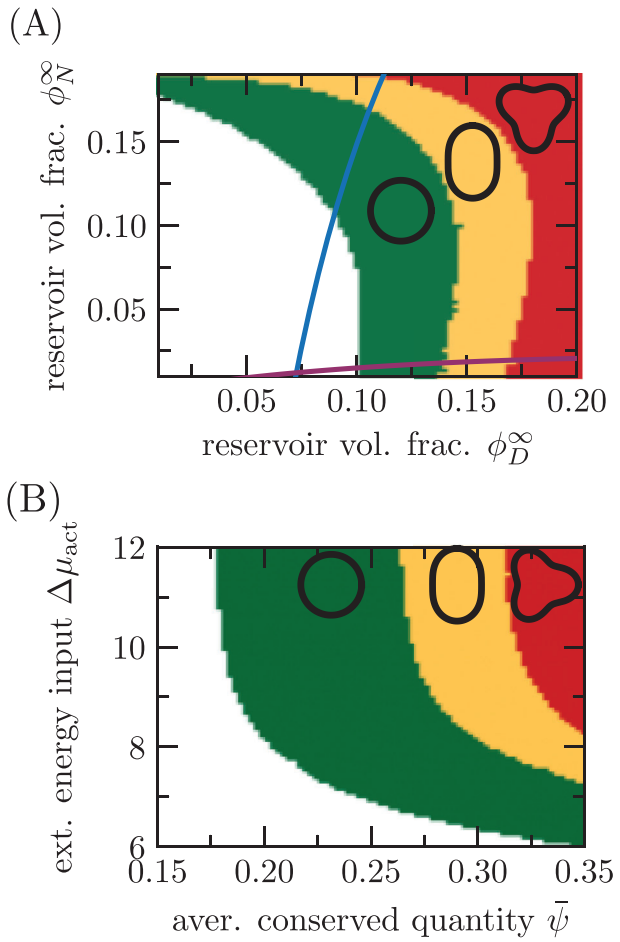

Figure 4. Shape stability diagrams for chemically active droplets for A) the boundary driven case and B) the bulk driven case. In the green area stationary droplets of spherical shape can exist. All shape perturbations decay. In the yellow area, the slowest $l = 2$ perturbation becomes unstable, thus droplets elongate. In the red area, additionally the slowest $l = 3$ mode become unstable. For the boundary driven case, we show the stability for a specific value of waste volume fraction of the reservoir, $\phi_W^\infty = 0.001$. Therefore, we can draw the chemical equilibrium line of reaction $\alpha = 1$ (purple) and the binodal line of these systems in the absence of chemical reactions (blue). Parameter values are given in Table C1 and Appendix C.

coexistence is shown as a solid blue line. In the absence of chemical reactions, droplets within the binodal region grow, while outside they shrink. Chemical reactions also permit the existence of chemically active droplets outside of the binodal region, where droplet material is constantly lost toward the reservoir. Under such nonequilibrium conditions, the volume fractions at the interface (governed by the binodal) differ from the values at large distances imposed by boundary conditions. The solid purple line indicates chemical equilibrium of reaction $\alpha = 1$, where the chemical rate r_α changes sign. For nutrient volume fractions above this line, droplet material is produced by the nutrient, while below this line, nutrient is produced.

Figure 4B shows the corresponding stability diagram for the bulk driven case as a function of the conserved density at infinity ψ^∞ and the active chemical free energy $\Delta\mu^{\rm act}$. The same regions of stability are indicated: stable spherical droplets green, unstable mode with $l = 2$ yellow and unstable mode with $l = 3$ red. Spherical stable droplets will typically divide when the conserved quantity is supplied, that is, the conserved density ψ^∞ is increased. Moreover, for increasing values of $\Delta\mu^{\rm act}$, the stability of active droplets becomes independent of $\Delta\mu^{\rm act}$. This is because almost all waste is turned over to nutrient by the chemical reaction $\alpha = 3$.

5. Energy, Mass, and Entropy Balance of Protocells

We now discuss energy and mass balance of stationary active droplets in the boundary driven case, where conserved quantities are only supplied at large distance. The fluxes of the conserved quantity ψ carry material associated with the growth and shrinkage of droplets. In a stationary case, these fluxes are zero. Nevertheless, the chemical reactions within the droplet lead to gradients of the chemical potentials, $\nabla\mu_i \neq 0$. At the same time, chemical reactions are also maintained out-of-equilibrium, corresponding to a nonvanishing Gibbs reaction free energy $\Delta\mu_\alpha \neq 0$. Both, chemical and diffusive fluxes give rise to a production of entropy according to Equation (25).

To discuss energy balance, we also consider heat. Heat is released by chemical reactions if the reaction enthalpy $\Delta h_\alpha > 0$ (exothermic), and is absorbed by chemical reactions if $\Delta h_\alpha < 0$ (endothermic). In addition heat is absorbed or released at the droplet interface (latent heat) for $\sum_i \boldsymbol{j}_i \nabla h_i > 0$ and $\sum_i \boldsymbol{j}_i \nabla h_i < 0$, respectively. Here, the sum is over all solute species.

Figure 5A–P presents four scenarios that differ in the heat release by reactions and the heat release at the interface. In all of the four scenarios, the imposed chemical potentials at the large distance start high for the nutrient, is lower for droplet material and lowest for waste, $\mu_N^\infty > \mu_D^\infty > \mu_W^\infty$, see chemical potential profiles in Figure 5A,E,I,M. This biases reactions $\alpha = 1$ and $\alpha = 2$ in the forward direction and diffusive transport and chemical reactions run in the same directions in all four scenarios. Correspondingly, the radial profiles of local entropy production $\dot{\Theta}$ is very similar in all four scenarios, see Figure 5B,F,J,N. Note that the entropy production rate $\dot{\Theta}$ jumps at the interface because the reaction rates r_α change discontinuously at the interface. The maxima of entropy production rate occur close to the interface since newly supplied material first reaches the droplet surface where it starts to react.

The first scenario of exothermic reaction and latent heat release at the interface is shown in Figure 5A–D. In addition to the profiles of chemical potentials and entropy production, it is characterized by profiles of molecular enthalpies h_i and total heat flux $\boldsymbol{J}_q = 4\pi r^2 \boldsymbol{j}_q$, see Figure 5C,D. The nutrient enthalpy inside the droplet $h_N^{\rm I}$ (blue) is larger than the waste enthalpy $h_W^{\rm I}$ (red), indicative of a net exothermic reaction from N to W. In addition, Figure 5C shows that at the interface $h_N^{\rm II} - h_N^{\rm I} > h_W^{\rm II} - h_W^{\rm I}$, corresponding to a net latent heat release. Here, the index I refers to the droplet phase and II to the phase outside. The release of heat at distance r corresponds to the slope of total heat flux $\mathrm{d}\boldsymbol{J}_q/\,\mathrm{d}r$. Heat release by chemical reactions corresponds to an increase of $\boldsymbol{J}_q$ inside the droplet, the contribution of latent heat is captured by a discontinuity of $\boldsymbol{J}_q$ at the interface.

There are three further additional scenarios are shown in Figure 5: Exothermal reactions with latent heat absorption at the

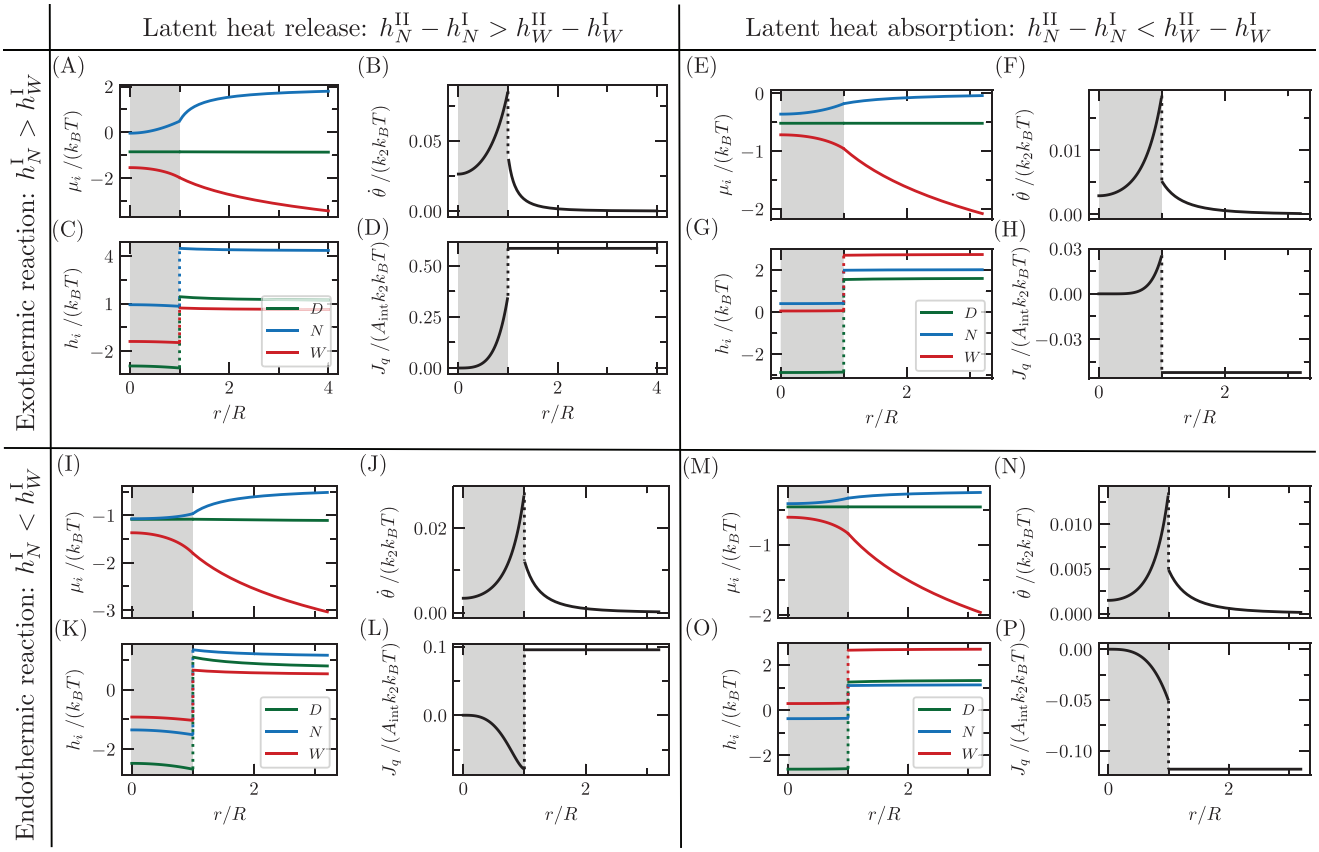

Figure 5. Energetics of active droplets. A,E,I,M) The profiles of chemical potentials for four different boundary driven stationary active droplets. B,F,J,N) Due to the constant driving, these stationary droplets are nonequilibrium steady states characterized by their entropy production. C,G,K,O) Despite similar profiles of chemical potentials, these four scenarios differ in their profiles of molecular enthalpies h_i. D,H,L,P) Thus the total heat flux $\mathbf{J}_q = 4\pi r^2 \mathbf{j}_q$ varies respectively. For simplicity, we have chosen ϕ_D^{∞} such that the current of droplet material vanishes outside of the droplet in the steady state. Thus there is no flux of the droplet material over the interface at stationary state, which would contribute to latent heat production or absorption. Parameter values are given in Table C1 and Appendix C.

interface Figure 5E–H, endothermal reactions with heat release Figure 5I–L and endothermal reactions with heat absorption Figure 5M–P. In the case of endothermal reactions, the enthalpy of the waste is higher than that of the nutrient, see Figure 5K,O In the case of latent heat absorption, J_q drops at the interface, such that the heat generated inside the droplet by exothermic reactions is not fully transported to the outside Figure 5H. Finally, in the case of endothermic reactions and heat absorption at the interface, the system takes up heat, which enters at large distances and is absorbed by reactions inside the droplet, Figure 5P. The droplet, therefore, acts as a cooling device, which in the case of finite heat conductivity would lead to lower temperatures inside the droplet compared to the outside.

6. Discussion

By combining the physics of phase separation and the thermodynamics of chemical reactions governing the law of mass action, we provide a theoretical framework for chemically active droplets. Such droplets have been proposed as models for protocells which are prebiotic, cell-like objects that could have emerged at the origin of life.[9–12] Chemically active droplets rely on phase separation leading to coexisting phases which organize chemical reactions that are maintained away from equilibrium. Using our framework, we discuss two cases how such droplets can be maintained away from equilibrium, see Figure 1: A) Droplets coupled to external reservoirs at the system boundary supplying nutrient and removing waste. In this case, detailed balance holds in the system and non-equilibrium conditions only enter via the reservoirs at the boundaries. B) Droplets driven by a chemical fuel in the bulk. In this case, detailed balance of the chemical reaction between nutrient and waste is broken in the bulk. Both cases (A) and (B) can exhibit nonequilibrium steady states with nonvanishing currents of energy and matter.

In our work, we discuss the balance of matter by introducing conserved densities and the nonconserved reaction extents. In addition, we consider the balance of energy. We show that the growth or shrinkage of a chemically active droplet is governed by fluxes of the conserved quantities at the droplet surface. We further show that the maintenance of nonequilibrium steady states is enabled by fluxes of the nonconserved reaction extents. From the point of view that active droplets represent simple models for protocells, the chemical reactions inside the droplets represent a simple metabolism.

In biology, metabolic processes are classified as anabolic or catabolic. Anabolic processes are considered to build complex components from smaller units by consuming energy, while catabolism typically describes the break-up of complex molecules to smaller units by which energy is released. The reactions in our models of protocells can capture such anabolic and catabolic processes. As an example, we can consider nutrient and waste to be simple molecules of high and low internal energy, respectively. Droplet material D would then represent more complex components. In such a setting, the reaction $N \rightleftharpoons D$ ($\alpha = 1$) corresponds to anabolic processes, while the reaction $D \rightleftharpoons W$ ($\alpha = 2$) corresponds to catabolic processes.

Our work highlights the different roles of conserved densities ψ_j and of non-conserved reaction extents ξ_α for protocell dynamics. This distinction between conserved and nonconserved densities is relevant not only for protocells, but also for biological cells. We can distinguish processes associated with mass and volume growth from processes that maintain nonequilibrium conditions even in the absence of growth. Growth processes in cells typically require the production of complex molecules by anabolic processes. Maintaining a cell away from equilibrium requires the supply of chemical fuels, such as ATP, via catabolic processes. Therefore, anabolism and catabolism can be related to growth and maintenance, respectively. In our formalism describing protocells, growth is related to the accumulation of conserved densities ψ_j, while maintenance is associated with the dynamics of nonconserved reaction extents ξ_α. Our work shows that maintaining reaction extents away from equilibrium is a hallmark feature of living systems.

A signature of the nonequilibrium state of living systems is the release of heat.[22] Our framework captures energy balance and heat exchange. Nutrients supply free energy via a high chemical potential as compared to waste $\mu_N > \mu_W$, which drives the system out-of-equilibrium. Typically, nutrient N is also a molecular energy carrier and waste W a low energy molecule which is reflected in molecular enthalpies ($h_N > h_W$). In this case, active droplets are exothermic and release heat, see Figure 5A–D. However, protocells could also be endothermic if the molecular enthalpy of waste exceeds that of nutrient ($h_N < h_W$). In this case, the droplet would absorb heat from the environment, see Figure 5M–P. The latent heat of phase separation at the interface also enters this energy balance. Latent heat can be either released or absorbed, which leads overall to four different scenarios shown in Figure 5. One of these scenarios shows that even if the droplet absorbs heat and appears to be endothermic, the reactions inside could still be exothermic, see Figure 5E–H. This shows that a measurement of overall heat absorption by an organism does not necessarily imply endothermic biochemistry, see[23,24]

Chemically active droplets can also divide. Division of chemically active droplets was suggested in theoretical works for liquid droplets, either by modulating surface tension using chemical gradients,[13] or via a dynamical shape instability studied in a minimal model.[14] Here, we have discussed shape instabilities leading to droplet division in multi-component mixtures motivated by protocells. In a binary system, chemical reactions have to convert droplet material D and solvent S, which phase-separate, into each other. We have shown that droplet division can occur in multi-component mixtures, when the solvent S that phase-separates from the droplet material D is not taking part in chemical reactions.

Our work is relevant for experimental studies of active droplets. Such experimental systems typically involve multiple components that undergo chemical reactions.[16–19] As our work shows, simply providing energy via a fuel is not sufficient to drive growth, because growth requires the accumulation of a conserved quantity. Similarly, cycles of droplet growth and division also requires the supply of a conserved quantity. These different roles of conserved densities for growth and nonconserved reaction extents for maintenance highlight the importance of energy and matter supply for chemically active droplets.

Appendix A: Free Energy

The chemical potentials given in Equation (5) are derived from the free energy

$$F = \int d^3x \left[f(\phi) + \sum_{i=1}^{M} \frac{\kappa_i}{2\nu_i} (\nabla \phi_i)^2 \right] \tag{A1}$$

with the Flory–Huggins type of free energy density

$$f = \sum_{i=0}^{M} \frac{k_B T}{\nu_i} \phi_i \log(\phi_i) + \sum_{\langle ij \rangle} \chi_{ij} \phi_i \phi_j + \sum_{i=0}^{M} \omega_i^0 \phi_i \tag{A2}$$

where $\phi_0 = 1 - \sum_{i=1}^{M} \phi_i$, and the sum over the pairs $\langle i, j \rangle$ include all possible combinations of different i and j, including the solvent. For simplicity, we have neglected contribution related to gradient in solvent volume fraction. Moreover, χ_{ij} is a matrix describing the molecular interactions with $\chi_{ii} = 0$ and ω_i^0 are the internal free energies. After replacing the solvent volume fraction and using the definition $\mu_i = \nu_i \delta F / \delta \phi_i$, we obtain

$$\mu_i = k_B T \log\left(\phi_i \phi_0^{-\nu_i/\nu_0} \right) + 1 - \frac{\nu_i}{\nu_0} - \kappa_i \nabla^2 \phi_i \tag{A3}$$

$$+\nu_i \sum_{j=1}^{M} (\chi_{ij} - \chi_{i0} - \chi_{j0}) \phi_j + \nu_i \chi_{i0} + \nu_i \omega_i^0 - \nu_i \omega_0^0 \tag{A4}$$

We can now identify the composition independent reference chemical potential

$$\omega_i = 1 - \frac{\nu_i}{\nu_0} + \nu_i \chi_{i0} + \nu_i \omega_i^0 - \nu_i \omega_0^0 \tag{A5}$$

and the exchange activity coefficient as stated in Equation (6).

Appendix B: Effective Description of a Single Active Droplet

The nonlinear, fourth-order partial differential equations (4) govern the spatial dynamics of concentration fields. To analyze the shape stability of active droplets, we derive an effective description for the dynamics of a single active droplet for the limit of a sharp interface. To this end, we linearize dynamic equations (4) leading for each component to two linear, second-order partial differential equations coupled via a moving boundary condition at the droplet interface, which we refer to as interface conditions in the following. For each time point, such nonlinear boundary conditions are solved by a set of volume fractions right inside and outside of the interface. These volume fractions serve as linearization points for the dynamic equations.

For the boundary driven case, we can solve for the interface dynamics considering a quasi-stationary limit. In particular, we use the stationary

solutions to the linearized equations and can solve for the slow interface dynamics. This slow dynamics is driven divergence-free currents of the conserved quantities. In the bulk driven case, we solve directly for the stationary positions of the interface. Due to the absence of divergence-free currents, using stationary solutions for the differential equations for the volume fractions automatically enforce a resting interface.

B.1. Spherical Symmetric Stationary Droplet

Linearizing Equation (4) around the volume fractions at the interface $\Phi_i^{\mathrm{I/II}}$, where I and II indicate the droplet phase and phase outside of the droplet, respectively

$$\partial_t \phi_i = \sum_j \left[D_{ij}^{\mathrm{I/II}} \nabla^2 \phi_j + k_{ij}^{\mathrm{I/II}} \left(\phi_j - \Phi_j^{\mathrm{I/II}} \right) \right] + c_i^{\mathrm{I/II}} \tag{B1}$$

where $D_{ij}^{\mathrm{I/II}} = D_{ij}(\Phi^{\mathrm{I/II}})$ are the diffusion constants introduced in Equation (8). Furthermore, linearizing the reaction rates r_i given in Equation (15) give the reaction coefficients

$$k_{ij}^{\mathrm{I/II}} = \frac{\partial r_i(\Phi_i^{\mathrm{I/II}})}{\partial \phi_j} \tag{B2}$$

and constant source or sink terms $c_i = r_i(\Phi_i^{\mathrm{I/II}})$. This constant only vanishes if the interface values correspond to a chemical steady state with $r_i = 0$.

We calculated stationary solutions to Equation (B1) for each phases in the case of a single droplet of radius R as a function of the volume fractions at the interface. The solutions for ϕ_i^{II} have to obey the boundary conditions at $r \to \infty$. For the boundary driven case, concentrations of nutrient, waste and droplet material are imposed, while for the bulk-driven case, no flux boundary conditions are used for all components. At the droplet center $r = 0$, the flux vanishes for each components and both cases. There are $2M$ unknown volume fractions at the interface. In addition, the interface velocity

$$v = \frac{\mathrm{d}R}{\mathrm{d}t} \tag{B3}$$

for the boundary-driven case, or the interface position R for bulk-driven case has to be determined via interface conditions, respectively. In total, this leads to $(2M + 1)$ unknowns.

Locally, at the droplet interface, we assume phase equilibrium. From this, we obtain M conditions from the balance of chemical potentials

$$\mu_i^{\mathrm{I}} = \mu_i^{\mathrm{II}} \tag{B4}$$

and one condition from the balance of the osmotic pressures right inside and outside of the droplet[15,25]

$$f^{\mathrm{I}} - f^{\mathrm{II}} = \sum_{i=1}^{M} \frac{\mu_i^{\mathrm{I/II}}}{v_i} \left(\Phi_i^{\mathrm{I}} - \Phi_i^{\mathrm{II}} \right) - \frac{2\gamma(\Phi^{\mathrm{I/II}})}{R} \tag{B5}$$

where γ denotes the surface tension γ. In multi-component mixtures, the surface tension γ varies for different phase equilibria along the binodal line. However, the method developed by de Gennes[26] can be generalized to multi-component mixtures for the case when $(\nabla \phi_D)^2$ is the dominant gradient contribution to the free energy (A1).

In systems without chemical reactions, global conservation laws of all M components dictate the selection of phase equilibra. In open systems, like in the considered boundary-driven case, the local conservation laws at the moving interface select specific phase equilibria. The remaining M conditions at the interface are given by

$$v\, e_r = \frac{j_i^{\mathrm{I}} - j_i^{\mathrm{II}}}{\Phi_i^{\mathrm{I}} - \Phi_i^{\mathrm{II}}} \cdot e_r \tag{B6}$$

This equations holds for each component for a moving interface. Thus, in total, we obtain the $(2M + 1)$ conditions at the interface.

In closed systems, like in our bulk-driven case with no-flux boundary conditions, local conservation laws at the interface of the reaction extents and global conservation laws of the conserved densities dictate the specific phase equilibria. Furthermore, in general, the interface cannot move when only stationary solutions of Equation (B1) are considered. In the absence of divergence-free currents, all currents of the conserved densities vanish in a stationary state. Thus, when the conserved density has different values in the phases, the droplet cannot grow.

Let us demonstrate the consequence of Equation (B6) in a ternary example with components A, B, the solvent S, and the chemical reaction $A \rightleftharpoons B$. In the stationary state for a closed systems $j_A^{\mathrm{I/II}} = -j_B^{\mathrm{I/II}}$. Using this relationship, and Equation (B6), we obtain

$$\frac{j_A^{\mathrm{I}} - j_A^{\mathrm{II}}}{\Phi_A^{\mathrm{I}} - \Phi_A^{\mathrm{II}}} = -\frac{j_A^{\mathrm{I}} - j_A^{\mathrm{II}}}{\Phi_B^{\mathrm{I}} - \Phi_B^{\mathrm{II}}} \tag{B7}$$

which can either be true when $j_A^{\mathrm{I}} = j_A^{\mathrm{II}}$ for a resting interface, or $\Phi_A^{\mathrm{I}} + \Phi_B^{\mathrm{I}} = \Phi_A^{\mathrm{II}} + \Phi_B^{\mathrm{II}}$ corresponding to a constant conserved density between the phases. Therefore, we can only solve for stationary interface position in general. Here, the remaining M equations consist out of C global conservation laws equations of the conserved variables

$$R^3 \psi_j^{\mathrm{I}} + (R_{\mathrm{sys}}^3 - R^3) \psi_j^{\mathrm{II}} = R_{\mathrm{sys}}^3 \bar{\psi}_j \tag{B8}$$

for finite systems with total system size R_{sys}. In the limit of infinite systems, this simplifies to $\psi_j^{\mathrm{II}} = \bar{\psi}_j$. From the local conservation laws of the $M - C$ reactions extents at the interface, we obtain

$$j_\alpha^{\xi,\mathrm{I}} = j_\alpha^{\xi,\mathrm{II}} \tag{B9}$$

Therefore, we obtain again $2M + 1$ equations, which determine the interface values and the stationary droplet radius R.

B.2. Stability of Spherical Droplets

In this section, we investigate the stability of spherical active droplets upon shape perturbations and study the relaxation dynamics of such perturbations

$$\phi_i^{\mathrm{I/II}}(r, \varphi, \vartheta, t) = \hat{\phi}_i^{\mathrm{I/II}}(r) + \delta\phi_i^{\mathrm{I/II}}(r, \varphi, \vartheta, t)$$

$$R(\varphi, \vartheta, t) = \hat{R} + \delta R(\varphi, \vartheta, t) \tag{B10}$$

where $\hat{\phi}_i(r)$ are the volume fraction profiles of the stable solutions and $\hat{R}$ is the stable droplet radius. We use the separation ansatz for the perturbations of the volume fraction values $\delta\phi_i^{\mathrm{I/II}}$, and the interface position δR of the form

$$\delta\phi_i^{\mathrm{I/II}}(r, \varphi, \vartheta, t) = \sum_{n,l,m} \epsilon_{nlm} o_{inl}^{\mathrm{I/II}}(r) Y_{lm}(\vartheta, \varphi) \mathrm{e}^{\tau_{nl} t}$$

$$\delta R(\varphi, \vartheta, t) = \sum_{n,l,m} \epsilon_{nlm} Y_{lm}(\vartheta, \varphi) \mathrm{e}^{\tau_{nl} t} \tag{B11}$$

Here, the index $n = 0, \ldots, \infty$, is related to the radial coordinate r, the index $l = 0, \ldots, \infty$, is related to the polar angle φ, and the index $m = -l, \ldots, l$ is

Table C1. Parameter values used in calculations shown in Figures 2–5.

	χ_{NS}	χ_{WS}	χ_{DN}	χ_{DW}	ω_D^0	ω_N^0	ω_W^0	$K_1 e^{-\omega_N^0}$	$K_2 e^{-\omega_D^0}$	$K_3 e^{-\Delta\mu^{act}}$	ϕ_D^∞	ϕ_N^∞	ϕ_W^∞	$\Delta\mu^{act}$	$\bar{\psi}$
Figure 2	1	0	0	1	10	20	0	0.025	0.001	–	0.08	–	0.0001	–	–
Figure 3A,B	−0.5	0.5	0	0	3	8	0	0.3	0.0088	–	0.08	0.15	0.001	–	–
Figure 3C	−0.5	0.5	0	0	3	8	0	0.3	0.0088	–	–	–	0.001	–	–
Figure 3D,E	−0.5	0.5	0	0	3	8	0	0.3	0.0088	0.008	–	–	–	9	0.25
Figure 3F	−0.5	0.5	0	0	3	8	0	0.3	0.0088	0.008	–	–	–	–	–
Figure 4A	−0.5	0.5	0	0	3	8	0	0.3	0.0088	–	–	–	0.001	–	–
Figure 4B	−0.5	0.5	0	0	3	8	0	0.3	0.0088	0.008	–	–	–	–	–
Figure 5A–D	1	0	−1	0	−0.8	4	1	0.3	0.0088	–	0.106	0.079	0.0001	–	–
Figure 5E–H	−1	0.5	0	0	−0.6	3	2.5	0.3	0.0088	–	0.100	0.107	0.0001	–	–
Figure 5I–L	1	0	−1	0	−0.8	1	1	0.3	0.0088	–	0.119	0.164	0.0001	–	–
Figure 5M–P	−1	0.5	0	0	−0.6	2	2.5	0.3	0.0088	–	0.115	0.182	0.0001	–	–

related to the azimuthal angle ϑ. The amplitude of each mode is given by ϵ_{nlm}, and its relaxation rate with τ_{nl}. Furthermore, Y_{lm} are the spherical harmonics. The radial problem reduces to M coupled Bessel equations with the solution given by

$$\varrho_{inl}^{\mathrm{I/II}}(r) = \sum_{k=1}^{M} A_k^{\mathrm{I/II}} \rho_{ikml}^{\mathrm{I/II}} \mathrm{b}_l^{\mathrm{I/II}}(\lambda_{knl}^{\mathrm{I/II}} r) \tag{B12}$$

where the component specific weight $\rho_{ikml}^{\mathrm{I/II}}$ and the inverse length-scale $\lambda_{knl}^{\mathrm{I/II}}$ are obtained from the M independent solution of the coupled problem for fixed n, l, m. The functions $\mathrm{b}_l^{\mathrm{I/II}}(x)$ are either modified spherical Bessel functions of first or second kind, according to the boundary conditions at $r = 0$ or $r \to \infty$. Boundary conditions at the interface fix the $2M$ unknown coefficients of $A_k^{\mathrm{I/II}}$ and the relaxation rate τ_{nl}. From the condition of phase equilibrium in linear order, we obtain

$$\sum_{j=1}^{M} \frac{\partial \mu_i^{\mathrm{I}}}{\partial \phi_j} \left(\partial_r \hat{\phi}_j^{\mathrm{I}}(\hat{R}) + \varrho_{jnl}^{\mathrm{I}}(\hat{R}) \right) =$$

$$\sum_{j=1}^{M} \frac{\partial \mu_i^{\mathrm{II}}}{\partial \phi_j} \left(\partial_r \hat{\phi}_j^{\mathrm{II}}(\hat{R}) + \varrho_{jnl}^{\mathrm{II}}(\hat{R}) \right) \tag{B13}$$

$$\frac{\gamma(\Phi^{\mathrm{I/II}})(l^2 + l - 2)}{\hat{R}^2} = \sum_{i=1}^{M} \frac{\phi_i^{I} - \phi_i^{\mathrm{II}}}{\nu_i}$$

$$\left(\sum_{j=1}^{M} \frac{\partial \mu_i^{\mathrm{I/II}}}{\partial \phi_j} \left(\partial_r \hat{\phi}_j^{\mathrm{I/II}}(\hat{R}) + \varrho_{jnl}^{\mathrm{I/II}}(\hat{R}) \right) \right) \tag{B14}$$

thus $M + 1$ conditions. The conservation law of each component at the interface, requires in linear order:

$$\tau_{nl}(\phi_i^{\mathrm{I}} - \phi_i^{\mathrm{II}}) = -\sum_{j=1}^{M} \Big[D_{ij}^{\mathrm{I}} \left(\partial_r^2 \hat{\phi}_j^{\mathrm{I}}(\hat{R}) + \partial_r \varrho_{jnl}^{\mathrm{I}}(\hat{R}) \right)$$

$$- D_{ij}^{\mathrm{II}} \left(\partial_r^2 \hat{\phi}_j^{\mathrm{II}}(\hat{R}) + \partial_r \varrho_{jnl}^{\mathrm{II}}(\hat{R}) \right) \Big] \tag{B15}$$

With this, we can obtain in total $2M + 1$ conditions at the interface, fixing the coefficients $A_k^{\mathrm{I/II}}$ and the relaxation rate τ_{nl}. When $\tau_{nl} > 0$, any small perturbation of the corresponding mode exponentially growths in linear order.

Appendix C: Parameter Choices

Here, we give the numerical values of the parameters used for producing the figures. For all figures, we have chosen $\nu = 1$, $\omega_S^0 = 0$, $\kappa_D = 1$, $\lambda = 1$, $k_B T = 1$, $\chi_{DS} = 3$ and $\chi_{NW} = 0$. As explained in Appendix B, $\kappa_N = \kappa_W = 0$ in the cases of the sharp interface limit. For the numerical simulation of Figure 2, $\kappa_N = \kappa_W = 1$. The remaining parameter vary for the different cases. Their values are given in **Table C1**. For Figure 2, we used a cubic lattice with $N = 128$ grid points in each dimension. The time points are given in terms of K_2.

Acknowledgements

Open access funding enabled and organized by Projekt DEAL.

Conflict of Interest

The authors declare no conflict of interest.

Keywords

active droplets, biological condensates, non-equilibrium fluids, phase separation, protocells

Received: March 25, 2022
Revised: June 4, 2022
Published online:

[1] A. A. Hyman, C. A. Weber, F. Jülicher, *Annu. Rev. Cell Dev. Biol.* **2014**, *30*, 39.
[2] Y. Shin, C. P. Brangwynne, *Science* **2017**, *357*, eaaf4382.
[3] S. F. Banani, H. O. Lee, A. A. Hyman, M. K. Rosen, *18*, 285.
[4] S. Boeynaems, S. Alberti, N. L. Fawzi, T. Mittag, M. Polymenidou, F. Rousseau, J. Schymkowitz, J. Shorter, B. Wolozin, L. Van Den Bosch, P. Tompa, M. Fuxreiter, *Trends Cell Biol.* **2018**, *28*, 420.
[5] C. Weber, T. Michaels, L. Mahadevan, *Elife* **2019**, *8*, e42315.
[6] J. Kirschbaum, D. Zwicker, *J. R. Soc. Interface* **2021**, *18*, 20210255.
[7] G. Bartolucci, O. Adame-Arana, X. Zhao, C. A. Weber, *Biophys. J.* **2021**, *120*, 4682.

[8] J. Bauermann, S. Laha, P. M. McCall, F. Jülicher, C. A. Weber, *arXiv:2112.07576* **2021**.
[9] J. B. S. Haldane, *Origin Life. Rationalist Annu.* **1929**, *148*, 3.
[10] A. I. Oparin, *The Origin Of Life*, Dover Publication, Mineola, NY **1952**.
[11] A. I. Oparin, A. G. Pasynskii, A. E. Braunshtein, *Origin of Life on the Earth*, Pergamon, Oxford **1957**.
[12] T. Hyman, C. Brangwynne, *Nature* **2012**, *491*, 524.
[13] N. Rashevsky, *Physics* **1934**, *5*, 374.
[14] D. Zwicker, R. Seyboldt, C. A. Weber, A. A. Hyman, F. Jülicher, *13*, 408.
[15] C. A. Weber, D. Zwicker, F. Jülicher, C. F. Lee, *Rep. Prog. Phys.* **2019**, *82*, 064601.
[16] F. Späth, C. Donau, A. M. Bergmann, M. Kränzlein, C. V. Synatschke, B. Rieger, J. Boekhoven, *J. Am. Chem. Soc.* **2021**, *143*, 4782.
[17] M. Abbas, W. P. Lipiński, J. Wang, E. Spruijt, *Chem. Soc. Rev.* **2021**, *50*, 3690.
[18] P. S. Schwarz, S. Laha, J. Janssen, T. Huss, J. Boekhoven, C. A. Weber, *Chem. Sci.* **2021**, *12*, 7554.
[19] K. K. Nakashima, M. H. van Haren, A. A. André, I. Robu, E. Spruijt, *Nat. Commun.* **2021**, *12*, 3819.
[20] D. Zwicker, *arXiv:2202.13646* **2022**.
[21] R. Rao, M. Esposito, *Phys. Rev. X* **2016**, *6*, 041064.
[22] J. Rodenfels, K. M. Neugebauer, J. Howard, *Dev. Cell* **2019**, *48*, 646.
[23] J. J. Heijnen, J. P. Van Dijken, *Biotechnol. Bioeng.* **1992**, *39*, 833.
[24] J.-S. Liu, I. W. Marison, U. von Stockar, *Biotechnol. Bioeng.* **2001**, *75*, 170.
[25] S. Safran, *Statistical Thermodynamics of Surfaces, Interfaces, and Membranes*, Westview Press, Boulder, CO **1995**.
[26] P. G. de Gennes, *Rev. Mod. Phys.* **1985**, *57*, 827.

Jonathan Bauermann studied physics at the University of Heidelberg and the Humboldt University Berlin. Currently, he is a Ph.D. student in Frank Jülichers group at the Max-Planck- Institut for the Physics of Complex Systems in Dresden.

Christoph A. Weber studied Physics at the Ludwig-Maximilian University in Munich and received his Ph.D. in theoretical physics on propelled particle systems in 2013 in the group of Prof. Frey. Then, as a postdoc, he joined the Max-Planck Institute for the Physics of Complex Systems in Dresden, performing research with Prof. Jülicher and Prof. Hyman on cytoplasmic phase separation. After that, he worked at Harvard John A. Paulson School of Engineering and Applied Science in the group of Prof. Mahadevan on pathogenic aggregation kinetics. In 2021, he became a full professor at Augsburg University, where he is in charge of the chair of Theoretical Physics II for Statistical Physics. His research group, "Mesoscopic Physics of Life," is devoted to the physics of intracellular organization and processes relevant to engineering life and the molecular origin of life.

Frank Jülicher studied Physics at the University of Stuttgart and RWTH Aachen University. He did his PhD work at the Institute for Solid State Research at the Research Center Jülich and received his PhD in 1994 from the University of Cologne. His postdoctoral work at the Simon Fraser University in Vancouver and the Institut Curie and ESPCI in Paris was followed by a CNRS research position at the Institut Curie in Paris in 1998. He has been a Director at the Max Planck Institute for the Physics of Complex Systems in Dresden and a professor of biophysics at the Technical University of Dresden since 2002. His research interests are theoretical approaches to active matter and the spatiotemporal organization of cells and tissues.